Tr. J. of Physics
23 (1999) , 751 – 763.
© TÜBİTAK

# Optimisation of the Tunable Wavelength Hot Electron Light Emitter

**Ali TEKE**
*Balıkesir University, Faculty of Art and Science,*
*Department of Physics 10100, Balıkesir-TURKEY*
**Naci BALKAN**
*University of Essex, Department of Physics,*
*Colchester, CO4 3SQ, UK*

Received 01.03.1999

**Abstract**

We report on the optimization of the hot electron tunable wavelength surface light emitting device developed by us. The device consists of a p-GaAs, and n-$Ga_{1-x}Al_xAs$ heterojunction containing an inversion layer on the p- side, and GaAs quantum wells on the n- side, and is referred to as HELLISH-2 ( Hot Electron Light Emitting and Lasing in Semiconductor Heterojunction). The device utilises hot electron **longitudinal** transport and, therefore, light emission is independent of the polarity of the applied voltage. In order to optimise the operation of the device a theoretical model that calculates the tunnelling and the thermionic components of the hot electron injection into the active region, was developed. The optimised structure, based on our model calculations is shown to have an operation threshold field about a factor of 3 lower than the earlier devices.

## 1. Introduction

A novel hot-electron light emitter, HELLISH-2 (Hot Electron Light Emission and Lasing In Semiconductor Heterostructures-Type 2) that can be operated for either single or multiple wavelength emission has been developed and widely reported by us [1-5]. In the current study we aim to, (i) present our model calculations to optimise device structure as to reduce the threshold field and enhance the emitted light intensity and (ii) investigate the performance of the optimized device

## 2. Structure of the devices

The devices, coded named, ES1 and QT919 were grown on Cr-doped semi-insulating

GaAs substrates oriented in the $< 100 >$ direction by MBE and MOVPE, respectively. Ohmic contacts were made by diffusing Au-Ge-Ni to all the layers. Figures 1(a) and 1(b) show the cross section the structure (a) and band edge profile (b) of the un-optimized device ES1. The structural parameters and the band edge profile of the optimized device, QT919 are shown in Figures 2(a) and 2(b), respectively. The structure consists of 3 $\mu$m p-GaAs buffer layer doped with Be, $N_A \sim 4.7x10^{16}\,\mathrm{cm}^{-3}$. Unlike the ES1 structure, QT919 has a 50 Å GaAs quantum well adjacent to p-n junction plane. Also the $Al_{0.33}Ga_{0.67}As$ barrier is much thinner than that in ES1. These two features are introduced as a result of our optimization studies as described below, to provide enhanced hot electron tunnelling from the QW into the inversion layer. The width of the rest of the QWs in QT919 is identical to those in ES1.

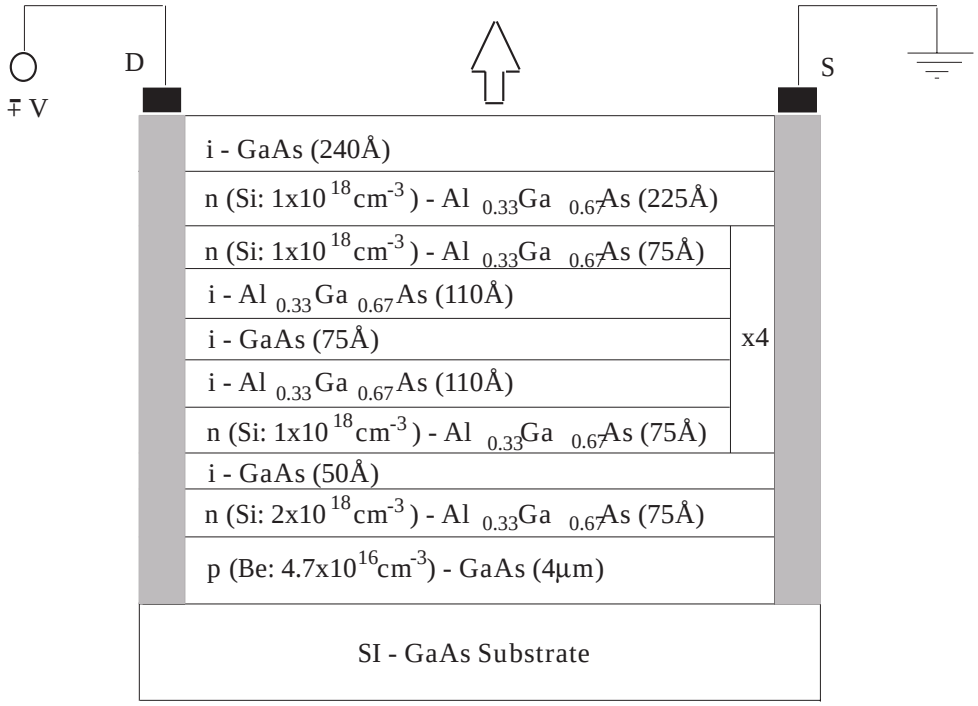


**(a)**

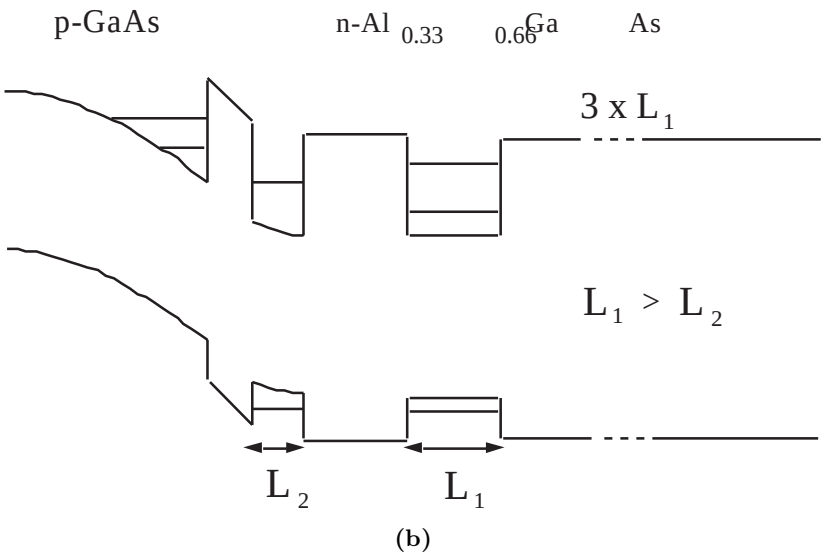


**Figure 1.** (a) The layered structure and (b) band edge profile of sample ES1. V is the applied voltage and arrow indicates the light emission from the surface and $L_1 = 75\mathring{A}$ is the quantum well width.

### 3. Device Operation

Figure 3 shows the schematics of potential profiles and the carrier dynamics involved in device operation for ES1 and QT919. When the electric field is applied parallel to the layers, the electrons in the quantum well adjacent to the junction plane are heated up to non-equilibrium temperatures $T_{e_1} > T_L$ and, transferred to the inversion layer via phonon-assisted tunnelling and thermionic emission [1-5].

The accumulation of excess negative charge in the inversion layer modifies the potential profile: The depletion region on the p-side of the junction is decreased as it were forward biased. The holes, therefore, which are initially away from the junction diffuse towards the junction plane. Thus the electron and hole wave functions overlap in the vicinity of inversion layer giving rise to a radiative recombination ($hv_1$) which corresponds to band-to-band transition in GaAs. As the field is increased injected hot electron current from quantum well to the inversion layer increases. Furthermore, the non-equilibrium electrons in the inversion layer, which also see the same external field, heat up to a temperature $T_{e_1} > T_L$ begin to occupy the higher energy states. Therefore, a high energy tail which is representative of a Maxwellian distribution is expected to develop in the EL spectra associated with the inversion layer transition. Because the emitted light is collected from the surface of the samples, photons from the inversion layer with energies greater than the $e1 - hh1$ energy separation in the quantum wells will be absorbed and re-emitted at energy ($hv_2$) corresponding to the $e1 - hh1$ transition in the quantum well. With increasing field, both the injected hot electron density in the inversion layer and

the occupancy of high energy states increases, so that more high energy photons become available for absorption in the wells. As a result, the intensity of re-emission from the quantum wells increases rapidly with increasing field for both samples.

The thermionic emission the current density is given by [6]

$$J_{ther}(T_e) = \frac{e}{4\pi^3}\int_v f(E)T(E)v_z dV, \tag{1}$$

where $dv = dk_x dk_y dk_z$(the volume element in momentum space in Cartesian co-ordinates) and is written as $dv = k_{\|}dk_{\|}d\theta dk_z$ in polar co-ordinates. $T(E)$ is the transmission coefficient for the single barrier case and $v_z$ is the component of the electron velocity perpendicular to the barrier .

$$v_z = \frac{\hbar h_z}{m^*} \quad \text{and therefore} \quad k_z dk_z = \frac{m^*}{\hbar^2}dE_z \tag{2}$$

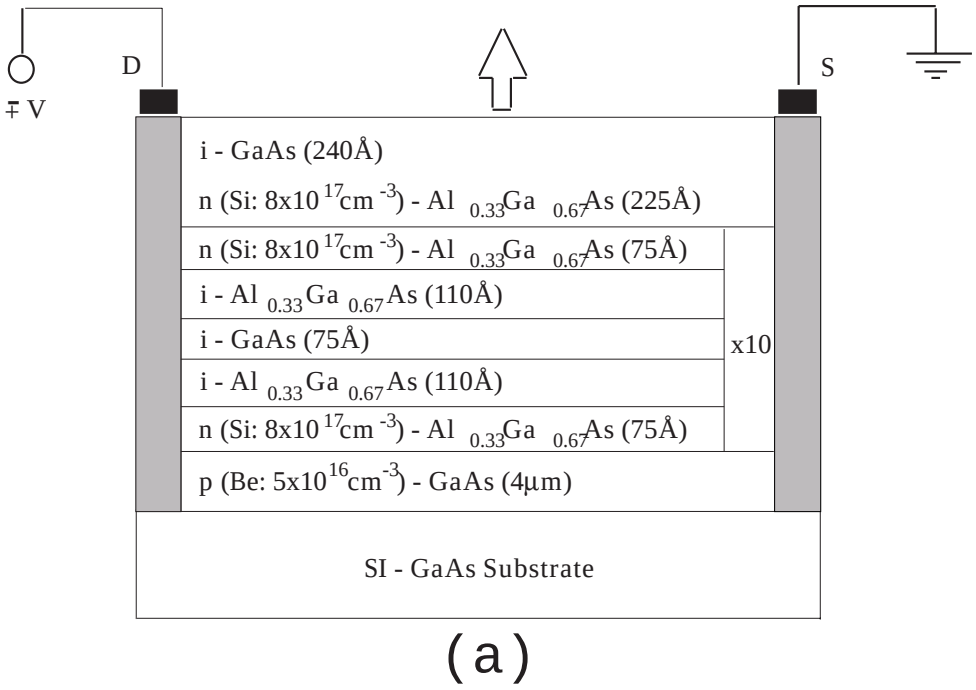


( a )

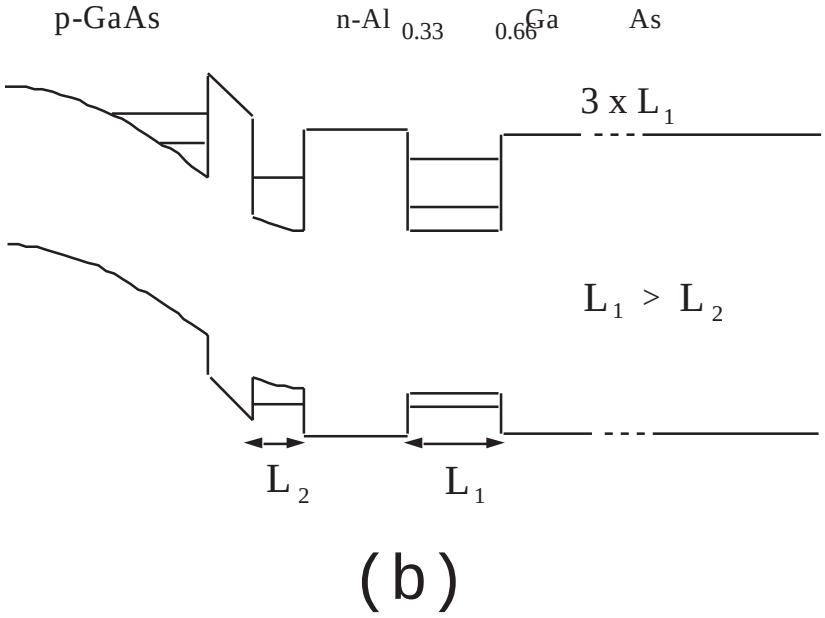


**Figure 2.** (a) The layered structure and (b) Band edge profile of the sample QT919. V is the applied voltage and arrow indicates the light emission from the surface and $L_1 = 75\mathring{A}$ and $L_2 = 75\mathring{A}$ are quantum well widths.

and the electron energy in the plane is

$$E_{\parallel} = \frac{\hbar^2 k_{\parallel}^2}{2m^*} \quad \text{and therefore} \quad k_{\parallel} dk_{\parallel} = \frac{m^*}{\hbar^2} dE_{\parallel}, \tag{3}$$

where is the plane wave vector and is written as $k_{\parallel}^2 = k_x^2 + k_y^2$. For simplicity, we can assume that transmission coefficient tends to unity as the electrons traverse the barrier ballistically. We can also assume that $E - E_F \gg k_B T$ and so we can apply Maxwell-Boltzmann statistics; then in cylindrical polar co-ordinate system equation (1) can be written in terms of energy as [6]:

$$J_{ther}(T_e) = \frac{em^*}{2\pi^3\hbar^3} \int_{v_b}^{\infty} \int_0^{\infty} \int_0^{2\pi} \exp\left\{ \frac{E_F - E_{\parallel} - E_z}{k_B T_e} \right\} dE_2 dE_{\parallel} d\theta. \tag{4}$$

Integration $\theta$ over $2\pi$ gives and integration over $E_{\|}$ gives $k_B T_e$. As a result, the thermionic emission current density is given by

$$J_{ther}(T_e) = \frac{em^*(k_b T_e)^2}{2\pi^3\hbar^3} \exp\left\{\frac{E_F - V_b}{k_B T_e}\right\} \tag{5}$$

where $E_F - V_b$ is the barrier between the Fermi level and inversion layer.

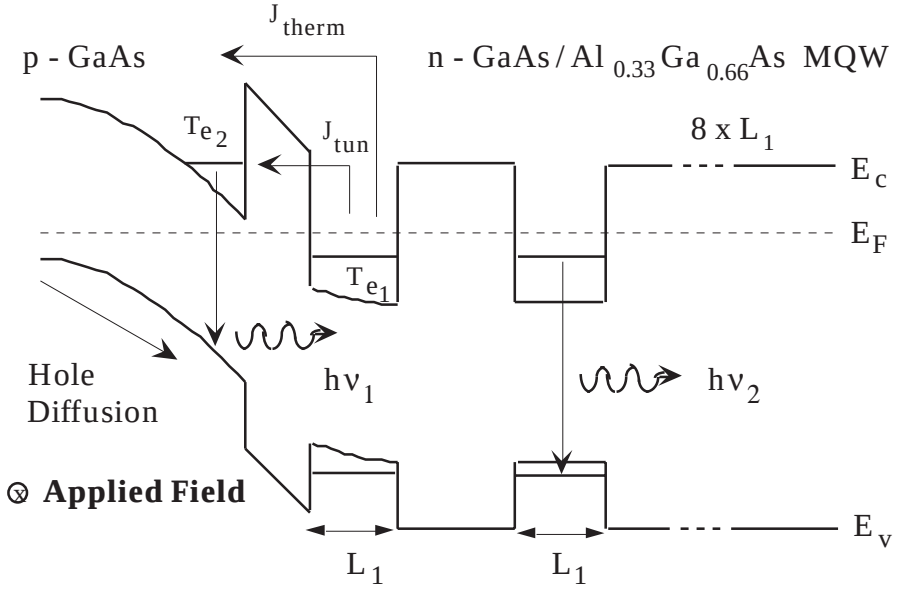


**Figure 3.** The conduction and valance band profile of the devices with an illustration of the carrier dynamics involved in device operation. $T_{e_1}$ and $T_{e_2}$ are the electron temperatures in the quantum well and in the inversion layer, respectively. $J_{ther}$ and $J_{tun}$ are the thermionic and tunneling components of the hot electron currents. The light emissions are also indicated. Electric field is applied parallel to the layers.

In the case of phonon-assisted tunnelling processes, electrons are injected from quantum well to the inversion layer by absorption of an LO phonon. (see P. J. Turley et al [7]). The temperature dependent tunnelling current density from quantum well to inversion layer is given by [7]

$$J_{tun}(T_e) = \frac{e}{4\pi^3\hbar}\int\left[1 - f\left(\mathbf{k}'_{\|}\right)\right]\mathbf{k}'_{\|}\mathbf{d}k'_{\|}\int_{-\pi}^{\pi}d\theta\int f(\mathbf{k}_{\|})\mathbf{k}_{\|}\mathbf{d}k_{\|}\beta^2(\mathbf{q}_{\|})I^2(\mathbf{q}_{\|})\delta(E_i - E_f + \hbar\omega), \tag{6}$$

where $f(\mathbf{k}_{\|})$ and $f(\mathbf{k}'_{\|})$ are the Fermi distribution function of electrons in the quantum well and in the inversion layer, respectively. $i$ and $f$ represent the initial and final electronic

state, and $\hbar w$ is the optical phonon energy, $\mathbf{k}_\parallel$, ($\mathbf{k}'_\parallel$) and $\mathbf{q}_\parallel$ are electron and phonon wave vectors in the plane of the well (inversion layer) respectively. $\theta$ is the angle between the incoming, $\mathbf{k}_\parallel$ and $\mathbf{k}'_\parallel$ the scattered, electron. $\beta(\mathbf{q}_\parallel)$ is the electron phonon coupling constant and is given by

$$\beta^2(\mathbf{q}_\parallel) = \frac{\gamma_c^2}{L(q_\parallel^2 + \alpha_n^2)}. \tag{7}$$

where

$$\gamma_c = \left[\frac{\hbar\omega e^2}{\varepsilon_0}\left(\frac{1}{\kappa_\infty} - \frac{1}{\kappa_0}\right)\right]^{1/2} \quad \text{and} \quad \alpha_n = q_z = \frac{n\pi}{L}, \tag{8}$$

where $\kappa_\infty$ and $\kappa_0$ are the high- and low-frequency dielectric constants, respectively. $q_z$ is the electron wave vector perpendicular to the plane and $L$is the quantum well width. Under the consideration of assumption which has been made for the overlap integral $I(\mathbf{q}_\parallel)$, in terms of energy over $\mathbf{k}_\parallel$ and $\theta$ equation (6) yields:

$$J_{tun}(T_e) = \frac{em^*\gamma_c^2 I^2(\mathbf{q}_\parallel)}{2\pi^2 L\hbar^3}\int_0^\infty \frac{dE'}{\left[\exp\frac{(E'-\hbar\omega+\Delta E-E_{F_w})}{k_B T_e}+1\right]\left[\exp\frac{(E_{F_{inv}}-E')}{k_B T_e}+1\right]} \times \frac{1}{\left[\frac{2\hbar^2\alpha_n^2 E\prime}{m^*} + \left(\frac{\hbar^2\alpha_n^2}{2m^*} - \hbar\omega + \Delta E\right)\right]^{1/2}}, \tag{9}$$

where $E_{F_w}$ and $E_{F_{inv}}$ are the temperature dependent Fermi energies in the well and in the inversion layer with respect to conduction band edge, respectively. $\Delta E$ is the energy difference between the confined states in the well and in the inversion layer. $m^*$ is the electron effective mass, and $\hbar$ is the reduced Plank constant. The overlap integral, $I$, is

$$I = \int \Psi^*_{inv}(z)u(z)\Psi_w(z)dz, \tag{10}$$

where $\Psi_w$ and $\Psi_{inv}$ are the unperturbated electron wave functions in the infinite well approximation in the well and the inversion layer, and $u(z)$ is the phonon displacement which is given by $u(z) = \cos(\alpha_n z)$. In our calculations, the z-dependence of $\Psi_{inv}$is not available in the well. Therefore, we make the approximation

$$\Psi_{inv} = \sqrt{T_{wi}}\Psi_w, \tag{11}$$

where $T_{wi}$ is the tunnelling transmission co-efficient.

In the model, carrier dynamics such as the hole injection, drift of carriers in the quantum well and in the inversion layer are not included. Nor do we include the recombination dynamics of the injected electrons with holes. We assume 100% internal efficiency where

all the electrons injected from quantum well to inversion layer recombine with holes. Under this assumption the calculated current densities from quantum well into inversion layer is shown in Figure 4 for sample ES1. In the calculations structural parameters, given in Table 1 are used.

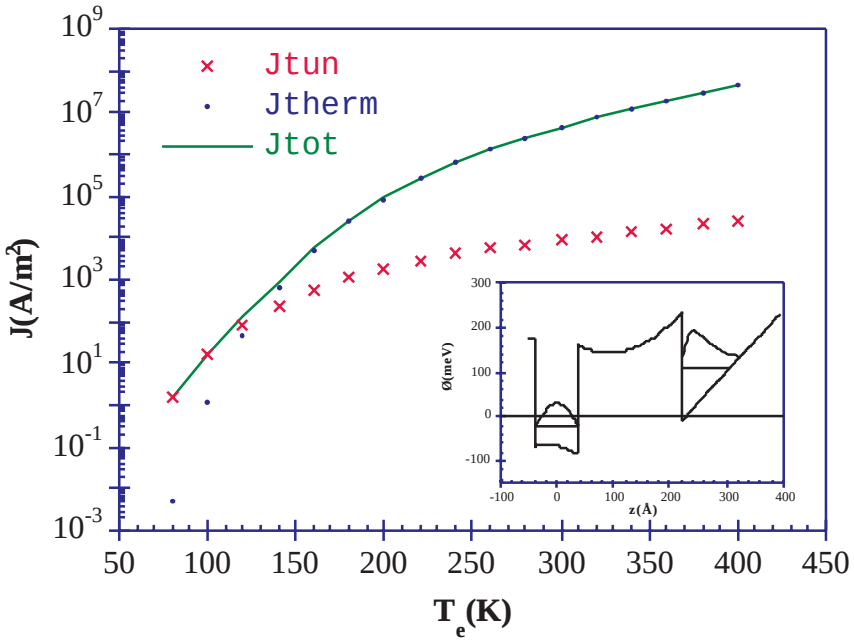


**Figure 4.** Temperature, $T_e$, dependence of the electronic currents, $J_{tun}$, $J_{therm}$ and $J_{tot}$ from quantum well to the inversion layer for ES1 where the parameters listed in Table 1. **Insert:** Calculated conduction band profile showing the electron wave functions in the well and in the inversion layer.

For ES1 the thermionic component of the total current dominates over the phonon-assisted tunnelling component. This is due to the large potential barrier width and large energy separation of the quantum well and the inversion layer first subbands, $\Delta E = E_{1_{inv}} - E_{1_w}$, as indicated in Table 1. Two parameters play an important role in determining the phonon-assisted tunnelling current in equation (9). The first one is the energy separation, $\Delta E$, which should be close to the optical phonon energy $(\hbar\omega)_{LO}$. The second one is the barrier width which should be reduced to increase the hot electron tunnelling currents from quantum well to the inversion layer. The energy separation between the first subbands in the quantum well and in the inversion layer can be altered simply by changing the p-doping density in the GaAs buffer layer. It is also possible to meet the first condition by changing the quantum well width adjacent to the junction plane. For the second condition we can simply reduce the barrier width between the quantum well and inversion layer. We designed the optimised sample QT919 by altering these

parameters as described above. We calculated both the tunnelling and the thermionic current density of the optimised sample QT919 and the result is shown in Figure 5. It is evident from the figure that phonon-assisted tunnelling current density is dominant over the thermionic emission one.

**Table 1.** Input parameters used in the program and output parameters in equilibrium for samples (a) ES1 and (b) QT919. Here: $N_d$ and $N_a$ are donor and acceptor concentrations, respectively. $L$ and $l_1$ are quantum well width and the separation width between the well and inversion layer, respectively. $E_{w_1}$ and $E_{inv_1}$ represent the first subband energy of the quantum well and that of the inversion layer, respectively, with respect to Fermi level set at zero energy. $\Delta E$ is energy difference between the first subbands of the quantum well and the inversion layer. $n_w$. and $n_{inv}$ are 2D electron concentrations in the well and in the inversion layer at equilibrium, respectively. $l_d$ and $l_a$ are the depletion lengths in the n-side and in the p-side of the junction, respectively.

| Input Parameters | | | | | | |
|---|---|---|---|---|---|---|
| $N_d(10^{18}cm^{-3})$ | | $N_a(10^{16}cm^{-3})$ | | $L(\mathring{A})$ | $l_1(\mathring{A})$ | |
| 0.8 | | 5.0 | | 75 | 185 | |
| output Parameters | | | | | | |
| $E_{w_1}(meV)$ | $E_{inv_1}(meV)$ | $\Delta E(meV)$ | $n_w$ $(10^{11}cm^{-2})$ | $n_{inv}$ $(10^{11}cm^{-2})$ | $l_d(\mathring{A})$ | $l_a(\mathring{A})$ |
| -19.82 | 111.89 | 131.91 | 5.44 | 0.0 | 273.01 | 2074.2 |

**(a)**

| Input Parameters | | | | | | |
|---|---|---|---|---|---|---|
| $N_d(10^{18}cm^{-3})$ | | $N_a(10^{16}cm^{-3})$ | | $L(\mathring{A})$ | $l_1(\mathring{A})$ | |
| 2.0 | | 4.7 | | 50 | 75 | |
| output Parameters | | | | | | |
| $E_{w_1}(meV)$ | $E_{inv_1}(meV)$ | $\Delta E(meV)$ | $n_w$ $(10^{11}cm^{-2})$ | $n_{inv}$ $(10^{11}cm^{-2})$ | $l_d(\mathring{A})$ | $l_a(\mathring{A})$ |
| -22.78 | 36.74 | 59.52 | 6.29 | 0.0 | 132.94 | 2291.9 |

**(b)**

## 4. Experimental Results

Figure 6(a) shows the EL spectra of sample ES1 for a number of different applied electric fields at 77K. The details of the measurements are described elsewhere [7-11]. The EL spectra for ES1 has a single peak at $hv_1 = 1.516eV$ at low fields. This peak is due to the band-to-band (e,h) transition in the inversion layer. As the electric field is increased, the spectra develops a high energy tail and the second peak at $hv_2 = 1.580eV$,

arising from the $el - hh1$ transition for the $L_z = 75\mathring{A}$ quantum wells is observed in the EL spectra. The intensity of the second peak grows faster than the first peak with the increasing field, eventually these two peak intensities become equal at an electric field around $F_{eq} = 1.2kV/cm$.

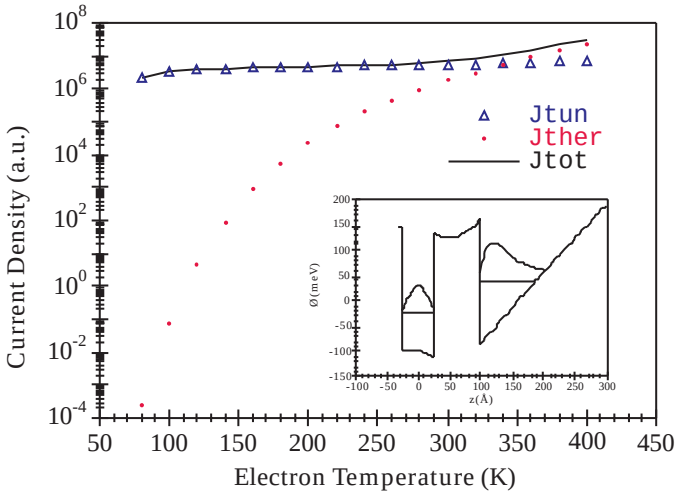


**Figure 5.** Temperature, $T_e$, dependence of the electronic currents, $J_{tun}$, $J_{therm}$ and from quantum well to the inversion layer for optimised device QT919 where the parameters listed in Table 1. **Insert:** Calculated conduction band profile showing the electron wave functions in the well and in the inversion layer.

Figure 6(b) shows the total integrated EL intensity as a function of applied electric field for ES1. The threshold field for an observable light emission is about $F_{thers} \sim 120$ V/cm. As explained above, thermionic emission is the dominant injection mechanism over the phonon-assisted tunnelling in the device (ES1), resulting in a lower injection of hot electrons at low fields. As a result, threshold field for the light emission is high. Above the threshold field integrated EL intensity increases with increasing applied field as expected from the enhanced electron injection into the inversion layer due to the increased carrier temperatures. Sample QT919 was designed with a similar structure to ES1 but was optimised as discussed above to reduce the threshold field for the light emission. EL spectra and the integrated EL intensity from this sample are depicted as a function of applied electric field at $T_L = 77$K in Figures 7(a) and 7(b). The EL spectra show the same characteristic as that observed from ES1. The reason for having two well resolved peaks at the low energy side of the EL spectra for sample QT919 compared with the single peak in sample ES1 has no significance, and is merely due to the difference in resolution of the experimental set-up. The field dependence of the integrated EL intensity of sample QT919, in Figure 7(b) also shows a behaviour similar to ES1. The threshold field for the light emission is, however, reduced by about a factor of three ($F_{threshold} \sim 40$ V/cm)

compared to that in ES1 because of dominant phonon-assisted tunnelling component of the injected current as our model calculations indicate.

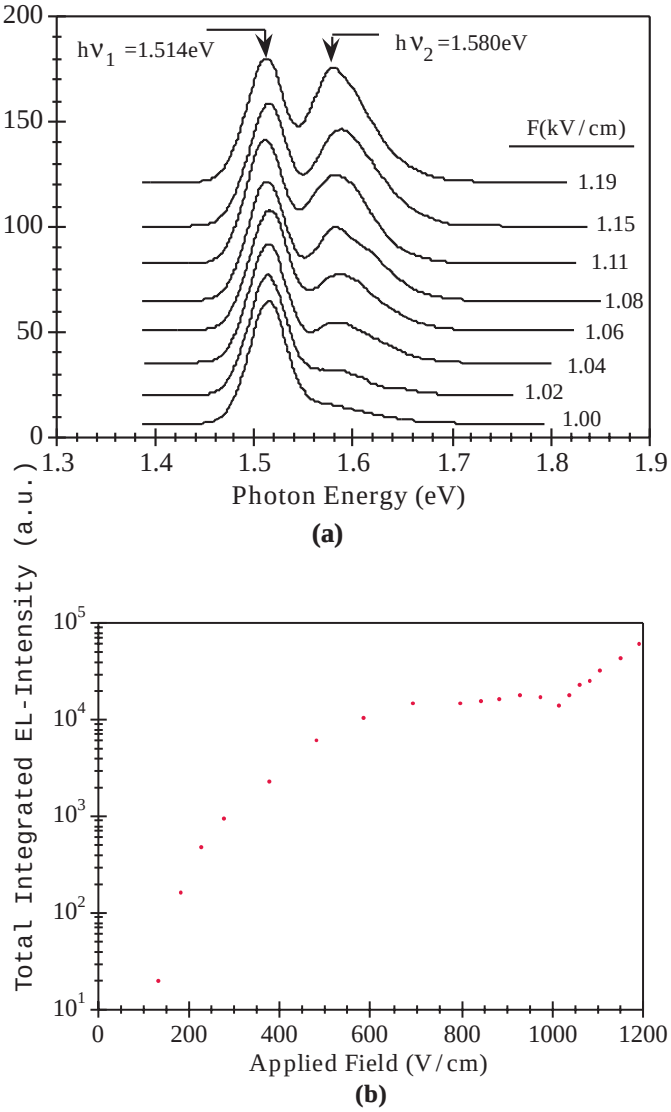


**Figure 6.** (a) Electroluminescence (EL) spectra taken at various electric fields and (b) total integrated EL intensity versus applied electric field at lattice temperature of $T_L = 77K$ for sample ES1.

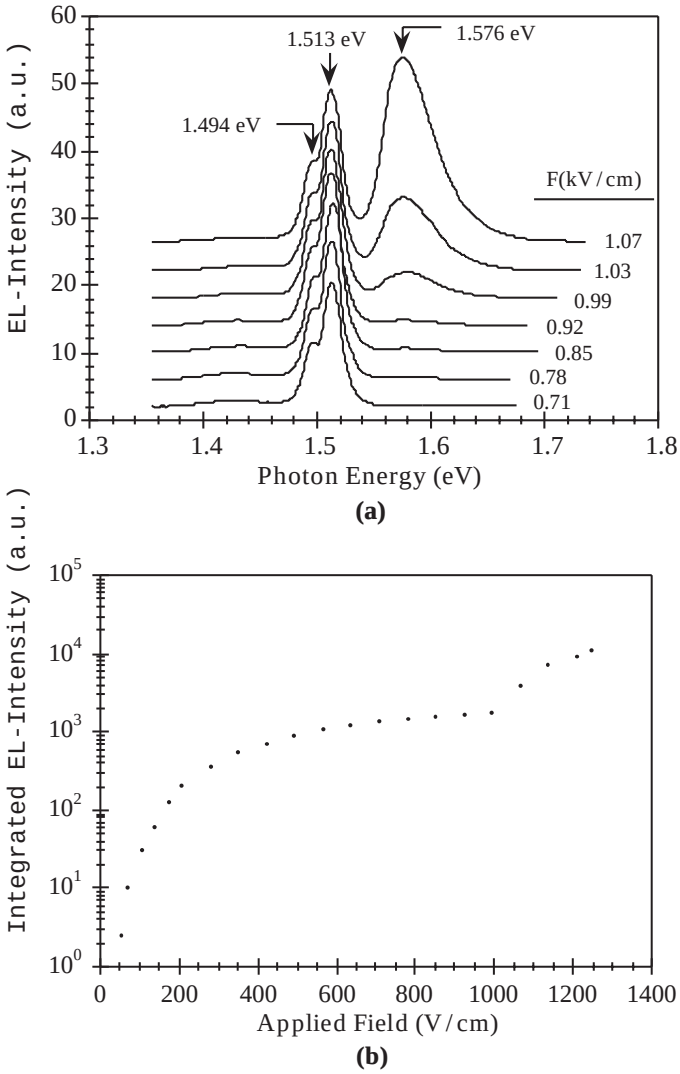


**Figure 7.** (a) Electroluminescence (EL) spectra taken at various electric fields and (b) total integrated EL intensity versus applied electric field at lattice temperature of $T_L = 77K$ for sample QT919.

## 5. Conclusions

In conclusion, we have demonstrated both theoretically and experimentally that the HELLISH-2 device can be optimized by a careful choice of the design parameters. The emitted light, in HELLISH-2 devices can be tuned from a single to multiple wavelength

operation by simple varying the applied voltage. The operation of these devices is based on carrier heating by means of the application of high electric fields. The emitted light intensity is therefore independent of the polarity of the applied voltage.

## References

[1] A. Straw, N. Balkan, A. O'Brien, A. da Cunha, R. Gupta and M. C. Arikan, Superlattices and Microstructures, 18, 1995, 33

[2] N. Balkan, A. Teke, R. Gupta, A. Straw, J. H. Wolter and W.Vleuten Appl. Phys. Lett. 67, 1995, 935

[3] R. Gupta, N. Balkan, A. Teke, A. Straw, and A. Cunha, Superlattices and Microstructures,18,1995, 45

[4] N. Balkan, A. da Cunha, A. O'Brien, A. Teke, R. Gupta, A. Straw, M. Ç. Arikan, in "Hot Carriers in Semiconductors", edited by K. Hess et al., Plenum Press, New York, 1996, 603

[5] A. Teke, R. Gupta, N. Balkan, J. H. Wolter and W. Vleuten, Semicond. Sci. Technol., 12, 1997, 314

[6] A. Straw, A. da Cunha, R. Gupta, N. Balkan and B. K. Ridley, Superlattices and Microstructures, 16, 1994, 173

[7] P. J. Turley, and S. W. Teitsworth, Phys. Rev. B 50, 1994, 8423